Soft Matter

Accepted Manuscript

ROYAL SOCIETY OF CHEMISTRY

www.rsc.org/softmatter

ARTICLE TYPE www. rsc.org/xxxxxx | XXXXXXXX

Self assembly of magnetic nanoparticles at silicon surfaces

Katharina Theis-Bröhl,*[a] Philipp Gutfreund,[b] Alexei Vorobiev,[c] Max Wolff,[c] Boris P. Toperverg,[d,e] Joseph A. Dura,[f] and Julie A. Borchers[f]

Received 26th February 2015, Accepted Xth XXXXXXXXX 20XX
First published on the web Xth XXXXXXXXXX 200X
DOI: 10.1039/b000000x

Neutron reflectometry was used to study the assembly of magnetite nanoparticles in a water-based ferrofluid close to a silicon surface. Under three conditions, static, under shear and with a magnetic field, the depth profile is extracted. The particles have an average diameter of 11 nm and a volume density of 5 % in a D_2O/H_2O mixture. They are surrounded by a 4 nm thick bilayer of carboxylic acid for steric repulsion. The reflectivity data were fitted to a model using a least square routine based on the Parratt formalism. From the scattering length density depth profiles the following behavior is concluded: The fits indicate that excess carboxylic acid covers the silicon surface and almost eliminates the water in the densely packed wetting layer that forms close to the silicon surface. Under constant shear the wetting layer persists but a depletion layer forms between the wetting layer and the moving ferrofluid. Once the flow is stopped, the wetting layer becomes more pronounced with dense packing and is accompanied by a looser packed second layer. In the case of an applied magnetic field the prolate particles experience a torque and align with their long axes along the silicon surface which leads to a higher particle density.

1 Introduction

Ferrofluids (FF) are colloidal suspensions of magnetic nanoparticles (NPs) with a diameter of a few nanometers. The particles are smaller than the minimum size of a magnetic domain and therefore they are expected to be in a mono-domain state[1,2]. Due to thermal motion the magnetic moments of the particles are randomly oriented in the absence of an external magnetic field and the liquid as a whole exhibits a paramagnetic behavior. Typically the particles are suspended in a carrier fluid such as oil, water, or others and are coated by long chain ligands. This geometry leads to a competition between magnetic and steric interactions resulting in strong correlations between magnetic and translational degrees of freedom. Both thermal motion and steric repulsion keep the ferrofluid stable with respect to agglomeration.

In an external magnetic field the magnetic moments of individual particles orient along the field lines, while dipolar interactions simultaneously lead to field-induced ordering[3]. This results, for example in magneto-rheological and other properties which are of strong interest as the viscosity sensitively depends on external magnetic fields[4]. In particular, under the influence of shear, a torque is applied to the particles, leading to a field-induced viscosity anisotropy, as has been observed in a ferrofluid based on nanodisc cobalt particles[5]. As a result of their unique field-dependent properties, magnetic liquids offer enormous potential for applications. Recent advances of ferrofluid research and application of magnetically controllable and tunable fluids in field such as optics, sensors, actuators, seals, lubrication, and static/dynamic magnetically driven assembly of structures are summarized in Ref.[6].

Recently several small-angle neutron scattering (SANS) studies probing the inter-particle correlation under the influence of external magnetic fields have been performed on a series of cobalt core/shell FF samples with Co concentrations ranging from 0.2 to 6 vol% and a particle size of 12 nm (core radius: 3.7 nm, ligand-shell thickness: 2.3 nm)[7,8]. With a magnetic field of 1 T applied to samples with Co concentrations above 1 vol%, pronounced magnetic anisotropy was observed. The data have been explained by the formation of hexagonal layers aligned with the normal to the plane perpendicular to the magnetic field but with no preferred orientation in the plane. For a diluted sample with 1 vol% Co no hexagonal planes were found but there was a strong indication for the presence of chain-like aggregates of particles aligned along the magnetic field. However, coexistence of chain segments with hexagonal ordered domains has been observed when the magnetic field was increased to 1 T[9]. The observed phenomena were explained by competing interactions between hard core repulsion, Van der Waals attraction and magnetic dipole-

[a] *University of Applied Sciences Bremerhaven, An der Karlstadt 8, 27568 Bremerhaven, Germany. Tel: +49 471 4823 471; E-mail: ktheisbroehl@hs-bremerhaven.de*
[b] *Institut Laue-Langevin, 71 Avenue des Martyrs, 38000 Grenoble, France.*
[c] *Division for Materials Physics, Uppsala University, 75120 Uppsala, Sweden.*
[d] *Institute for Solid State Physics, Department of Physics, Ruhr-University Bochum, D-44780 Bochum, Germany.*
[e] *Petersburg Nuclear Physics Institute, 188300 Gatchina, Russia.*
[f] *NIST Center for Neutron Research, 100 Bureau Drive, Gaithersburg, MD 20899-6102, USA.*

dipole interaction[8]. For small dipolar interaction the formations of either chains or chain segments may be favored as shown by rescaled mean sphere approximation modeling of competing repulsive and attractive interactions[10]. However, if dipolar interaction exceeds a critical value, a transition from the uniaxial to a lamellar ordering should occur, with almost close-packed in-plane structures, as shown by recent molecular dynamics studies.[11,12]

The appearance of magnetic-field induced changes of viscosity under shear stress was observed in 1969 in diluted suspensions of anisotropic shaped cobalt particles with a size of a few tens of nanometers at concentrations below 1 vol%[13]. Theoretical explanations of this effect are based on the concept of the constraint of free rotation of the particles in a shear flow due to the influence of an external applied field[14,15]. When a magnetic field is applied, a tendency for magnetic moments to orient parallel to the magnetic field direction is expected. Assuming the magnetic moment in each particle is fixed to the long axis, the particles will tend to align along the direction of the field. Shear flow, however, applies a mechanical torque on each particle due to the viscous friction. This causes a misalignment of the magnetic moments away from the magnetic field direction. Without a magnetic field the particles under shear flow are able to rotate freely but with an applied magnetic field, free rotation of the particles in the flow is hindered. As a result, a magnetic torque is expected to realign the magnetic moments along the magnetic field leading to an increase of viscosity in the FF.

Other SANS investigations also take into account shear flow and have studied magneto-viscous effects in ferrofluids by using a specially designed rheometer[16]. Shear rates up to $200\ s^{-1}$ and magnetic fields up to 200 mT have been applied to magnetite and cobalt-based ferrofluids. The magnetite-based ferrofluids show only relatively weak changes under the influence of magnetic field and shear indicating the formation of short chains. For cobalt-based ferrofluids, however, stronger effects occur with evidence for formation of a chain-like structure under the influence of magnetic field and shear flow. This observation is also supported by molecular dynamic simulations[17].

As a further control parameter, the interaction of a ferrofluid with a solid interface was investigated. Studies via optical experiments[18] and theoretical calculations[19] describe the existence of a surface-induced ferrofluid wetting layer on a glass substrate. Strong off-specular x-ray scattering was detected when studying the interaction of a ferrofluid of 11 nm sized superparamagnetic particles with a silicon surface[20]. It was explained to be due to capillary waves, related to the presence of aggregates of particles, with fractal dimensions in the vicinity of the silicon surface.

Neutron reflectivity (NR) studies of a very dense FF (with a concentration of 9 vol% and 5.5 nm size Fe_3O_4 particles in D_2O) in contact with a horizontal Si/SiO_2 surface show very interesting features. Without a magnetic field, a dense wetting double-layer at the SiO_2 surface develops within 1 h. Applying DC magnetic fields up to 10 mT leads either to short-range ordering when the magnetic field is parallel to the surface or to a long-range ordering in nanoparticle (NP) sheets adjacent to the Si/SiO_2 interface when the magnetic field direction is perpendicular to the SiO_2 surface[21]. The layering at the interface was found to be a very slow process and for a field applied perpendicular to the surface long-range ordering extending up to 30 layers into the FF was observed only after 48 hours.

In the present study we investigate the interactions of ferrofluids with a solid interface under the influence of both magnetic field and shear by using a shear cell in a vertical geometry. Measurements using a commercial water-based FF with 10 nm sized magnetite particles with an oleic acid based ligand dispersant are presented in this paper. This type chosen represents the most common type of ferrofluids and is close to what is used in industry. Neutron reflectivity was employed for getting insight into the out-of-plane structural ordering of the magnetic nanoparticles on a Si/SiO_2 surface, as well as insight into the characteristics of the organic layers between the nanoparticle cores. As each ferrofluid is a complicated system characterized by certain parameters such as concentration, particle type, size and distribution, ligand type, polarities etc. and as interactions with a solid interface also depend on the interface itself, the phenomena observed may not occur in exactly the same way in another FF system. However, certain trends of wetting and packing, for example, are transferable to similar ferrofluid systems and provide a basis for understanding these complex systems.

From previous studies it is known that magnetite particles with an oleic acid dispersant in water are always stabilized with a ligand double layer[22]. This is visualized in Fig. 1. The length of the oleic acid molecule is 2 nm. It is bent due to an unsaturated C=C bond in the middle resulting in a deformable shell. With a single layer the shell would be hydrophobic and thus unstable. However, the coating can be stabilized by excess free surfactant molecules forming a double layer membrane shell around the particle. The excess oleic acid is needed for a dynamic exchange with the outer shell around the particles. Otherwise the particles lose the outer shell relatively quickly. Our neutron investigations reveal that the surfactant shells coating the nanoparticles play a key role in stabilizing the nanoparticle wetting layers in this FF system.

These measurements set the stage for a wide range of studies into fundamental magnetic interactions on the nanoscale. From a basic science perspective this may serve as a tool to test interactions of magnetic domains of various sizes, strengths, and separations. This will be of particular value in validating nanomagnetic modeling. From an applied perspective, understanding the rheology and surface interactions of fer-

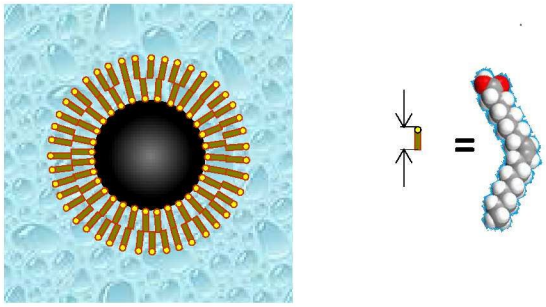

Fig. 1 (Color online) Schematic visualization of the double layer of oleic acid present around the magnetic core in water stabilizing the dispersion. The bent molecule has a length of 2 nm.

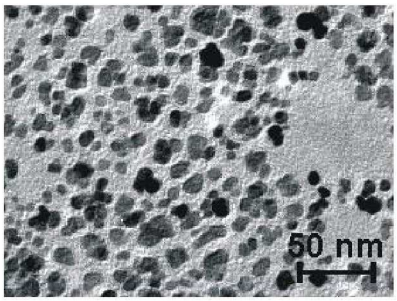

Fig. 2 TEM image taken from the magnetite nanoparticles.

rofluids will help extend the range of ferrofluid application. No measurements to date have determined the surface interactions of ferrofluids in the presence of flow and magnetic field with angstrom level precision as was performed in the present study.

2 Experimental

2.1 Sample

The commercial water based FF was supplied by Liquids Research Limited* and prepared by wet chemical precipitation[24]. The particles are magnetite, Fe_3O_4, which has been confirmed via x-ray powder diffraction. The nominal particle size is 10 nm with an oleic acid based ligand dispersant[24] which adds a shell with a thickness up to several nm in water. SQUID measurements show saturation at around 50 mT with a magnetic moment of about 0.06×10^{-3} Am^2 (= 0.06 emu).

To get information about the size distribution and the shape of the nanoparticles, transmission electron microscopy (TEM) was performed. Fig. 2 shows a TEM image from which can be seen that the particles are not completely spherical. The particle diameter was estimated from the square root of the particle area in the image. The same mean particle diameter has been determined using the Feret's diameter, which is also know as the maximum caliper. In this treatment, the longest distance between any two points along the selection boundary of the particle is taken and averaged [23]. The average particle diameter was thus determined to be (11.1 ± 3.6) nm with a bimodal size distribution. The 30% variation is typical for technical ferrofluids. Fits to small angle neutron scattering measurements (SANS) on a similar ferrofluid sample (see Fig. 3) reveal that the average diameter of the nanoparticles

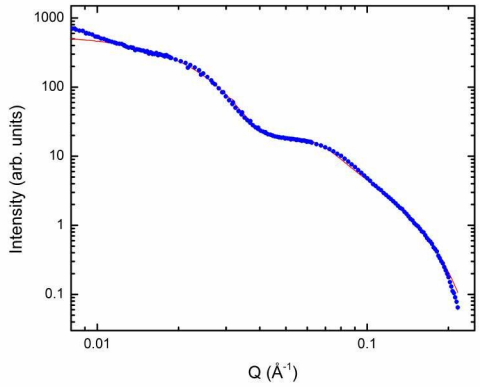

Fig. 3 Reduced SANS data taken from a similar ferrofluid and fit to a core-shell model.

in the ensemble is (10.6 ± 0.3) nm with a dispersity of 27% which is comparable to the TEM results. (Note that the SANS measurements were performed on the NG7 instrument at the NIST Center for Neutron Research.)

To decrease incoherent background scattering and for increasing the contrast for the neutron scattering experiments, most of the H_2O was exchanged to D_2O. The ferrofluid was determined to contain 70.5 vol% D_2O and 4.6 vol% of magnetite particles, in addition to the ligands and the residual H_2O. In order to estimate the missing volume fraction of oleic acid and H_2O, a simple hard sphere model was used. For the model it was assumed that the ligands form a spherical double shell of 4 nm thickness (see above) around a spherical Fe_3O_4 core of 11 nm (derived from the average particle diameter as results of the TEM measurements and the neutron data, see below). Neglecting the small amount of excess oleic acid in solution with this model and with the known concentration of the Fe_3O_4 cores of 4.6 vol%, the ligand content in the ferrofluid is estimated to be around 19.1 vol%. Combining these volume fractions and the known scattering length densities (SLDs), corresponding to the number density times the scattering length, of

* Certain products are identified to foster understanding, which does not imply recommendation or endorsement by the National Institute of Standards and Technology, nor does it imply that the materials or equipment identified are necessarily the best available for the purpose.

the oleic acid shell and the Fe_3O_4 cores, one can calculate the SLD of the water mixture to be $Nb_{D_2O/H_2O} = 5.81 \cdot 10^{-4} nm^{-2}$ and thus the ratio of D_2O to H_2O to be ~92.4:7.6 (see also Table 1).

As a solid interface a Si(100) crystal with dimensions of 80x50x10 mm^3 with one side polished was used. The silicon was carefully cleaned assuming that this procedure already provides a hydrophilic surface. It was assembled into a flow cell designed for neutron reflectivity measurements. In contrast to the investigation described in Ref.[21], the flow cell was oriented vertically in order to avoid nanoparticle sedimentation (due to gravity) on the Si surface. A similar flow cell is described in Ref.[26]. The liquid volume inside the cell was 70x40x1 mm^2.

2.2 Neutron scattering experiments

Neutrons, which can deeply penetrate in to materials, are either specularly reflected from variations of the mean optical potential in the surface normal direction or scattered in off-specular directions due to in-plane fluctuations of the potential, within the neutron coherence volume. Reflectometry essentially gives the depth profile of the mean optical potential averaged over the coherence volume of the neutron beam, which is large, on the order of 100 μm in the $x-$ direction[27–29].

The NR measurements where carried out on the reflectometer D17 at the Institut Laue Langevin (Grenoble, France) in time-of-flight mode using neutrons in the wavelength range between 2.2 Å and 27 Å. The wavelength resolution varied between 1 % and 2.5 % in the investigated q-range and the angular resolution was fixed to 2.4 % (both FWHM). The data were recorded by using two angles of incidence, namely 0.8° and 2.4°. The beam footprint on the sample was fixed to 40 x 60 mm^2. Details about the instrument are provided in Ref.[30]. The magnetic field was applied by using permanent plate-shaped magnets leading to an in-plane magnetic field in the sample center of 11 mT. The magnetic field was slightly higher closer to the magnets reaching up to 15 mT at the top/bottom part of the sample.

The collimated neutron beam penetrates the edge of the Si crystal and undergoes reflection at the internal interfaces (see Fig. 4). The reflectivity data were background corrected and fitted to a theoretical model profile by using a least squares routine with a Parratt formalism[31].

For determining the optimal number of fitting parameters the Bayesian Information Criteria, *BIC*,

$$BIC = (n-k)\chi^2 + k\ln(n) \quad (1)$$

were used with n being the total number of data points for the measurement, k the total number of fitting parameters, and χ^2 represents the reduced χ^2 statistic of the fit[32]. The optimal number of layers used for the fit is determined by the lowest *BIC* number. A neutron beam is incident through the silicon crystal. The top layer in the stack is the native SiO_2 layer with a thickness of (1.0 ± 1.0) nm and a SLD of $3.97 \cdot 10^{-4}$ nm^{-2} determined from a fit of the system $D_2O/SiO_2/Si$ and held fixed in fits to the data with the ferrofluid. The assumed layer structure is shown in Fig. 5 (a). The fit gives results for the thickness, roughness and SLD of each layer. For comparison, the bulk SLD values of the components of the ferrofluid are given in Table 1. The first layer in the model above the native oxide, is a layer (# 1) which is assumed mainly to consist of the oleic acid (OA) additive which is included in the ferrofluid to build up the ligand shell around the magnetic particles. The second layer (# 2) is expected to be a particle wetting layer consisting of magnetite cores, with some shell material between them and also some D_2O/H_2O. The ligand shell on the opposite side of the particles forms an additional layer (# 3), which, like layer # 1, has a lower SLD than layer # 2. It is also expected that a transition region between the wetting layer and the bulk ferrofluid builds up, which is modeled as layer # 4. Additional layers are included if necessary. Finally, the SLD of the ferrofluid bulk (FF bulk), together with its roughness are varied during fitting †[27,33].

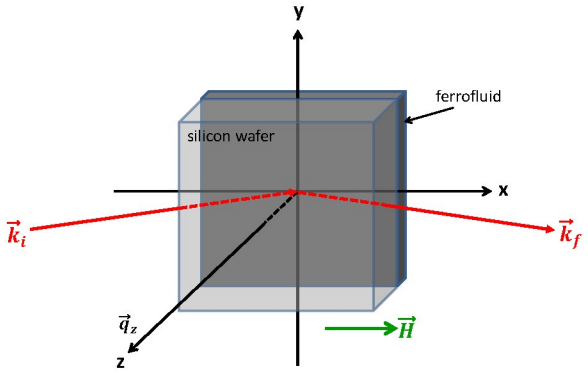

Fig. 4 (Color online) Sketch of the experimental setup showing the incident and reflected neutron (k_i, k_f) and the sample assembly. q_z is the wave vector momentum transfer perpendicular to the interface.

3 Neutron Reflectivity results

Neutron reflectivity measurements were performed under different conditions. First, shear was applied to the ferrofluid as it was pumped through the flow cell with a volumetric flow rate of $Q = 1000$ ml/min corresponding to a shear rate of $\dot{\gamma} = 3Q/(4d^2w) = 312.5\ s^{-1}$ for the flow through a rectangular cross-section for a gap width of $w = 4$ cm and a gap height of $d = 1$ mm. Second, the flow was stopped and a mea-

† The package uses the super-iterative algorithm[28].

Table 1 Bulk SLD values of the components of the ferrofluid and other materials as calculated by using Ref.[35].

Material	Function	Concentration c	Nuclear SLD Nb [10^{-4}nm^{-2}]
Components of the ferrofluid:			
Ferrofluid particle (19.4% Fe_3O_4/80.6% OA)	core/shell	0.237	1.41
Fe_3O_4	core	0.046	6.91
OA (oleic acid)	shell	0.191	0.08
Water (92.4% D_2O/7.6% H_2O)	solvent	0.763	5.81
D_2O	solvent 1	0.705	6.33
H_2O	solvent 2	0.058	-0.56
Ferrofluid (composed from above)		1.000	4.76
Silicon wafer:			
Si	wafer		2.07
SiO_2	native oxide		3.97

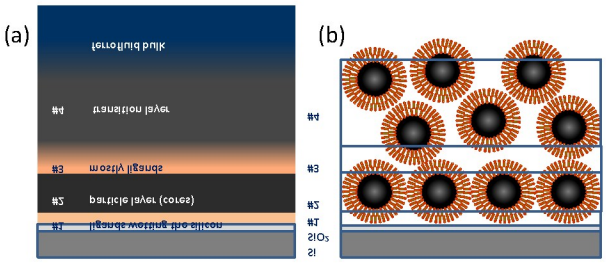

Fig. 5 (Color online) Model of layers for the superstructure which was assumed for performing fits to the reflectivity data. Schematic layer model (a) and hypothetical particle ordering within the layers # 1-4 (b).

surement in a static condition was taken. Third, a magnetic field of 11 mT was applied parallel to the silicon surface in static conditions.

3.1 Static case in zero field

The measurement taken without shear and without magnetic field is shown in Fig. 6. In the left diagram of Fig. 6 $R \cdot q_z^4$ is plotted as function of q_z and uncertainties are $\pm$ one standard deviation. The measured reflectivity shows pronounced deviations from the Fresnel curve, $R \propto q_z^{-4}$. The best fit to the data, with $\chi^2 = 1.16$, is shown as a solid line in Fig. 6. The resulting SLD profile is plotted at the right hand side of Fig. 6. As mentioned above, the optimal number of layers used for the fits was chosen by using the *BIC*-number (eq. 1). In all static measurements the *BIC* number was smallest when using 4 layers in between the SiO_2 layer and the FF-bulk as proposed by the model in Fig. 5. (The SLD values obtained from the fits to the data are given in Table 2). The best fitted SLD profile can provide quantitative information about the ferrofluid particles and their interfacial ordering.

Layer # 1 corresponds to the portion of the ligand shell separating the Fe_3O_4 particles from the substrate. From the fits to the data, layer # 1 has $Nb_{\#\,1} = 0.90 \cdot 10^{-4}$nm^{-2} and a thickness of (3.4 ± 1.2) nm. This value is close to the thickness of a double layer of oleic acid molecules which is expected to form around the magnetic particles. Assuming that this layer consists only of oleic acid and the D_2O rich water mixture and using the measured SLD of layer # 1 and the known SLDs of oleic acid and the water mixture (see Table 1), one can calculate that layer # 1 consists of 86% oleic acid and 14% water by volume. Fig. 7 depicts the ordering of particles in a wetting layer in a densely packed six-fold arrangement. In Fig. 7(a) the top view and in Figs. 7(b) and (c) side views of such a layer are shown. This ratio of oleic acid to water in layer # 1 as observed from our measurements is higher than could be derived from the model of an intact bilayer shown in Fig. 7(b) in which the oleic acid volume fraction is only 39%. However, due to the attraction of oleic acid to the polar surface, one can assume a dense bilayer of oleic acid at the SiO_2 as shown in Fig. 7(c). The portions near the Fe_3O_4 particles are shared as part of its bilayer shell with additional oleic acid bilayers fill the gap. The exact calculation of the water content of layer # 1 in this model depends on the packing density of the bilayer attached to the SiO_2 and how it deforms to fill the cavities between the bilayer shells around the Fe_3O_4 particles.

Layer # 2 is expected to contain the particle cores of the wetting layer. The best fits to the data resulted in a thickness of $t_{\#\,2} \approx (10.9 \pm 1.1)$ nm and a nuclear SLD of $Nb_{\#\,2} = 2.55 \cdot 10^{-4}$nm^{-2} for this layer. The thickness of this layer agrees very well with the average particle core diameter derived from TEM (see above). The SLD of this layer is explained by assuming closed packed spherical particles with a six-fold sym-

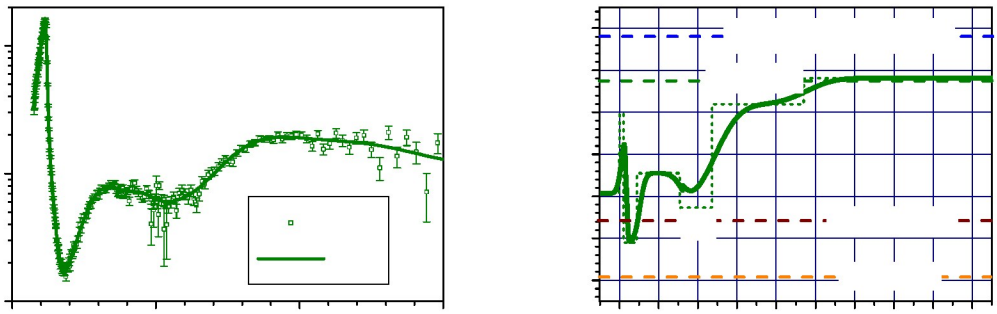

Fig. 6 (Color online) NR data taken in static conditions without applying a magnetic field. Left: Plot of $R \cdot q_z^4$ as function of q_z. The solid lines represent fits to the data. Right: Profile of nuclear scattering length density plotted as function of distance from the Si (100) surface determined from results of the least square fitting routines applied to the reflectivity data.

metry (the wetting layer) as is visualized in Fig. 7 in top and side view. For the calculation of the SLD of this layer (depicted by the rectangle in figure 6), the ligand shell above and below the planes tangent to the spherical particles were excluded, and the volume fraction of the three components between these planes were determined to be: 20% core material, 61% shell material and 19% D_2O/H_2O. This gives an SLD of $2.58{\cdot}10^{-4}\mathrm{nm}^{-2}$. This value is in very good agreement with the fit to the data for which the SLD is $\mathrm{Nb}_{\#\,2} = 2.55 \cdot 10^{-4}\mathrm{nm}^{-2}$ and indicates that indeed a densely packed layer of magnetic particles is formed at the solid boundary.

Layer #3 contains the ligand bilayer on the other side of the particles (away from the substrate) plus the ligand from another perhaps more disordered particle layer above it. The largest thickness of this layer that would be consistent with close packed planes is found for A-A stacking which is twice the length of a ligand bilayer, or around 8 nm. This thickness would also be consistent with the case for a less densely packed particle layer that is incommensurate with the particles in layer # 2. The fits to the data yield a thickness of (8.3 ± 2.1) nm which is in good agreement with this value. The SLD of layer # 3 was determined to be $\mathrm{Nb}_{\#\,3} = 1.73 \cdot 10^{-4}\mathrm{nm}^{-2}$. This value is higher than the measured SLD of layer # 1 but lower than the theoretical value of $2.31 \cdot 10^{-4}\mathrm{nm}^{-2}$ corresponding to 61% water content, which was calculated for layer # 1 in the hard shell model, Fig. 7(b), i.e. for a double ligand sub-layer from a densely packed particle wetting layer adjacent to a solid surface (which also corresponds to A-A hexagonal plane stacking). The much lower SLD can only be explained by an excess of oleic acid, since the SLD of both Fe_3O_4 and the water mixture is greater than the measured values. While greater oleic acid content would be expected for A-B hard shell stacking, this would also correspond to a layer thickness that is smaller than twice the shell thickness. However the opposite is observed. This excess oleic acid content likely is caused by a concentration of the excess oleic acid from solution that was not bound to the Fe_3O_4 particles in the densely packed region. Assuming no particle cores to be within this layer the ligand content can be determined to be 71 % and the D_2O/H_2O content to be 29 %.

Layer # 4 is the transition region between the wetting layer and the bulk ferrofluid. The fitted thickness is 23.4 nm and the SLD is $\mathrm{Nb}_{\#\,4} = 4.19 \cdot 10^{-4}\mathrm{nm}^{-2}$ (see Fig. 6). This SLD is much larger than that calculated for a densely packed layer including ligands (corresponding to layers # 1, # 2 and half of layer # 3) which is $\mathrm{Nb}_{\#\,1-\#\,3} = 3.34 \cdot 10^{-4}\mathrm{nm}^{-2}$. This result indicates that the particles in the transition layer are not closely packed and more water is found in the transition layer. However it is still slightly less than the SLD of the bulk ferrofluid, ($\mathrm{Nb}_{\mathrm{FF-bulk,exp}} = 4.81 \cdot 10^{-4}\mathrm{nm}^{-2}$) indicating that there is either slightly greater than bulk-like attraction between the particles (with a particle concentration of 9% compared to 4.6% in the bulk fluid), or an excess of unbound oleic acid in this region.

Furthermore, the shape of the SLD in Fig. 6 shows a plateau-like behavior at $z \sim$35 nm in depth which points to the formation of a distinct second layer, which, however, is not as closely packed as the wetting layer and even may consist of two A-B stacked single layers.

3.2 Static case with magnetic field

The evolution of reflectivity after applying a magnetic field of 11 mT parallel to the silicon surface and perpendicular to the neutron beam is shown in Fig. 8. The best fits to the data

Table 2 Results of the fits to the NR data concerning thickness, roughness and nuclear SLDs and taken under static conditions and under shear without applying a magnetic field .

Layer	without shear $\chi^2 = 1.16$			with shear $\chi^2 = 1.66$		
	Thickness t [nm]	Roughness Δt [nm]	Nuclear SLD Nb [10^{-4}nm^{-2}]	Thickness t [nm]	Roughness Δt [nm]	Nuclear SLD Nb [10^{-4}nm^{-2}]
SiO_2	1.0	1.0	3.97	1.0	1.0	3.97
# 1	3.4	1.2	0.90	3.2	0.5	1.12
# 2	10.9	1.1	2.55	15.0	1.1	3.17
# 3	8.3	2.1	1.73	2.8	0.9	3.44
# 4	23.4	5.0	4.19	12.2	3.2	5.15
FF-bulk	-	5.6	4.81	-	3.2	4.80

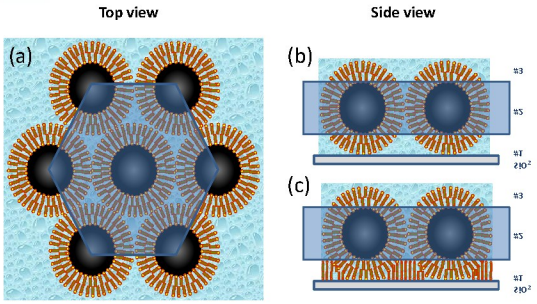

Fig. 7 (Color online)(a) Ordering of particles in a wetting layer in densely packed six-fold arrangement, (b) a model assuming intact bilayers, and (c) a model assuming that a bilayer of oleic acid wets the SiO_2 substrate and is also part of the bilayer surrounding the particle.

are shown as solid lines in Fig. 8 left and the corresponding SLD profiles are plotted in the right of Fig. 8. In Table 3 the parameters used for the fits to the data are given.

As in the static, zero-field case, the model with 4 layers (# 1-4) in between the SiO_2/Si-substrate and the ferrofluid bulk resulted in the smallest *BIC*-numbers and therefore was used to fit the data. Since the SLD profile is seen to evolve with time incrementally from the static case, the same interpretation of the layers is assumed, consisting of a particle wetting layer and a transition region between the wetting layer and the ferrofluid bulk.

In the first layer # 1 consisting of the surfactant bilayer and some D_2O/H_2O, the thickness remains at 3.4 nm after 2 h and 8 h and is fit to a slightly higher value of 3.7 nm after 20 h (which is still within the error bars of ± 1.0 nm). The SLD, however, increased to values between $Nb_{\#\,1} = 1.28 \cdot 10^{-4}\text{nm}^{-2}$ and $1.42 \cdot 10^{-4}\text{nm}^{-2}$ corresponding to an oleic acid content of 79-77 vol% and a water content of 21-23 vol% compared to 14 vol% water in the static, zero-field case. The volume expansion of this layer is roughly equal to the increased water content.

When a magnetic field is applied, the thickness of layer # 2 representing the cores, continuously decreases with time to a value of 8.7 nm, which is 2.2 nm, or $\sim 20\%$ less than the thickness obtained without applying the magnetic field. The SLD continuously increases with time, to a value of $Nb_{\#\,2} = 3.95 \cdot 10^{-4}\text{nm}^{-2}$ at 20 h.

To explain this behavior the real shape and the broad size distribution of the particles must to be taken into account (see Fig. 2). A decreased thickness can be explained by two different scenarios. In the first scenario, the particles experience a torque due to the applied field and orient with their long axis along the field, which was applied parallel to the silicon surface. This situation is visualized in model 2 of Fig. 9 assuming the simplest, elliptical, shape for anisotropic particles. This picture is in contrast to model 1 of Fig. 9 in which particles with an average spherical shape are shown, corresponding to the random orientation of the particles in the absence of an applied field. This reorientation of the particles with their major axis in the plane explains the reduction of thickness of layer # 2 and is consistent with its increased SLD by the increased volume fraction of the Fe_3O_4 which has a high SLD. The reorientation of the particles is observed to be a slow process, requiring roughly 20 hours until full alignment.

In a second scenario, the thickness reduction might be explained by an exchange of particles in layer two with preferential selection of smaller particles from the 30% size distribution. In such a case, however, the Fe_3O_4 volume fraction of the nanoparticles wetting the surface would decrease, while the shell thickness would not change. Therefore, the SLD for layer # 2 would decrease if the hard spheres are densely packed. With a particle diameter of 8.7 nm and a ligand shell thickness of 4 nm an SLD of $Nb_{\#\,2} = 2.22 \cdot 10^{-4}\text{nm}^{-2}$ can be calculated for this scenario. This model, however, disagrees with the results of the fits to the data which show an increased SLD, favoring the first scenario in which asymmetric Fe_3O_4 particles re-orient in the applied field.

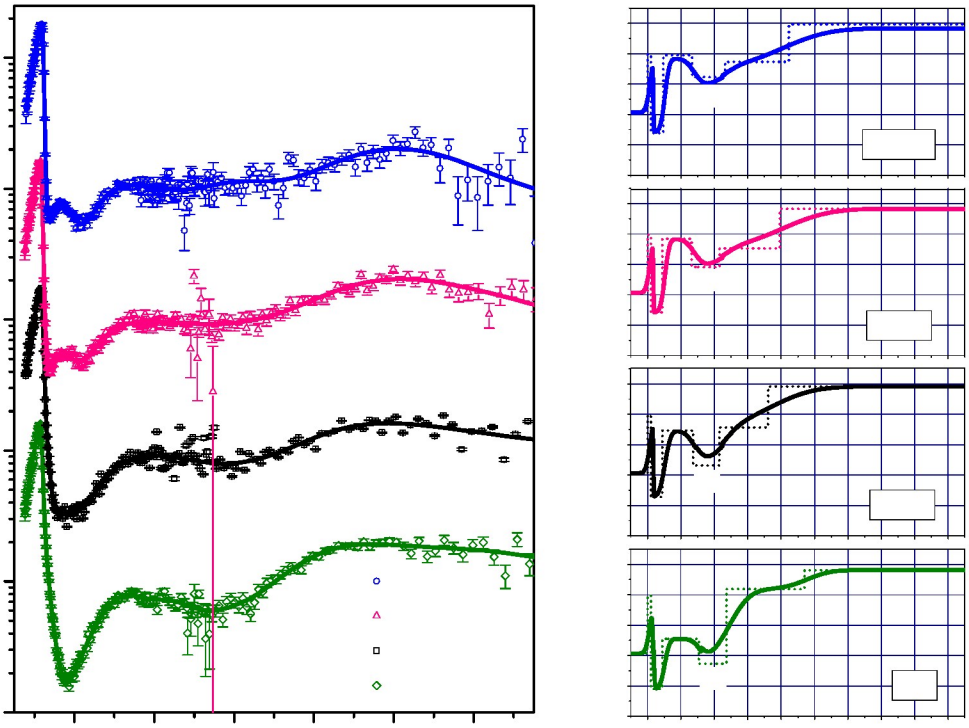

Fig. 8 (Color online) NR data taken before (green symbols) and during applying a magnetic field of 11 mT parallel to the Si(100) for 2 h (black symbols), 8 h (pink symbols) and after 20 h (blue symbols). Left: Plot of $R \cdot q_z^4$ as function of q_z. The solid lines represent fits to the data. Right: Profile of nuclear scattering length densities plotted as function of distance from the Si(100) surface determined from results of the least square fitting routines applied to the reflectivity curves.

Table 3 Results of the fits to the NR data concerning thickness, roughness and nuclear SLDs obtained under static conditions when applying a magnetic field of 11 mT.

Layer	after 2 h $\chi^2 = 1.4$			after 8 h $\chi^2 = 1.6$			after 20 h $\chi^2 = 2.3$		
	t [nm]	Δt [nm]	Nb [10^{-4}nm^{-2}]	t [nm]	Δt [nm]	Nb [10^{-4}nm^{-2}]	t [nm]	Δt [nm]	Nb [10^{-4}nm^{-2}]
SiO_2	1.0	1.0	3.97	1.0	1.0	3.97	1.0	1.0	3.97
# 1	3.4	1.0	1.28	3.4	1.0	1.42	3.7	1.0	1.39
# 2	9.2	1.4	3.47	8.8	1.1	3.84	8.7	1.2	3.95
# 3	7.9	2.5	2.32	8.4	2.1	2.91	10.8	1.5	3.23
# 4	14.6	4.5	3.57	18.0	4.1	3.53	18.1	3.3	3.73
FF-bulk	-	9.9	4.92	-	10.9	4.83	-	10.5	4.96

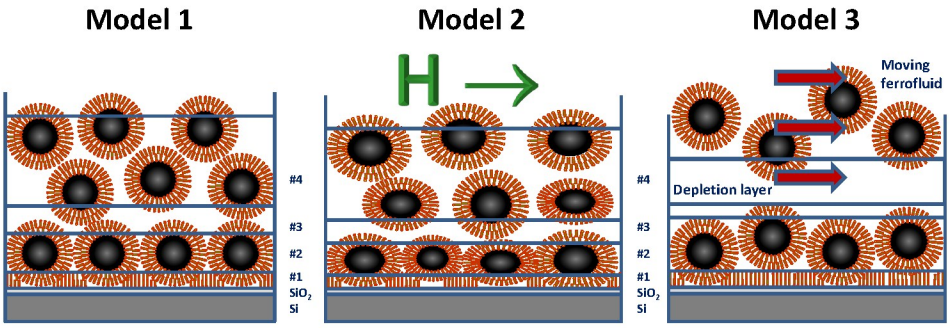

Fig. 9 (Color online) Models for the layering of the nanoparticles close to the silicon surface. The particles form a densely packed wetting layer at the surface which consists of layer # 1 which mostly is ligand material, a densely packed layer #2 containing the cores and ligands between them and a layer # 3 which contains ligands and some core material. All layers contain D_2O/H_2O in addition. Layer # 4 is the transition region between the wetting layer and the bulk of the ferrofluid which is not as densely packed as the wetting layer. In Model 1 spherical shaped particles are assumed, in Model 2 the case of an applied field is assumed with elliptical shaped particles aligned with their long axes in field direction parallel to the silicon surface, and in Model 3 the case under shear is visualized in which a depletion layer was found between the wetting layer and the moving ferrofluid.

Layer #3 containing the ligand material from the first and second particle layers reaches a thickness of 10.8 nm after 20 h in the magnetic field. This is a thickness increase of roughly 2 nm relative to the zero-field case. Since an increased thickness probably contains more water, its SLD would increase, which agrees with the fits to the data.

In the applied magnetic field, the transition region layer # 4 initially decreases in thickness and then expands with time. Since the thicknesses of the lower layers are also changing, layer # 4 ends at roughly the same distance from the substrate (60 nm) as in the static, zero-field case. However, as can be seen when comparing the fitted models at $t = 0$ and $t = 20$ h in Fig. 8, the SLD profile has a slightly different behavior in the transition region. The plateau region is much less pronounced when a field is applied, and the SLD changes more gradually. Nevertheless, the SLD value at around 35 nm depth, where the plateau occurs in the static zero field case, remains roughly the same in the applied field. Furthermore the SLD of layer # 2, the first particle layer, also approaches this value, as seen in Fig. 8 and the SLD values for layers # 4 and # 2 in table 3. Therefore, it can be assumed that in a field the second particle layer remains more densely packed than the bulk ferrofluid with density similar to the zero-field case, though it is not as pronounced. The increase in the SLD of the first particle layer thus can be explained, in part, by an increase in water content, consistent with that observed in layers # 1 and # 3.

The fitted SLD values of the bulk ferrofluid varies between $Nb_{FF} = (4.81...4.96) \cdot 10^{-4}\text{nm}^{-2}$ for the static cases with and without magnetic field with no specific trend. These values are within the uncertainty and agree with the value of $Nb_{FF,th} = 4.81 \cdot 10^{-4}\text{nm}^{-2}$ determined from the zero-field data.

3.3 Zero field case with applied shear

In the case of shear, the general layer composition is similar to the static zero-field case as is visualized in model 3 of Fig. 9. As can be seen in in the SLD curve in Fig. 10 for the case of shear, again a particle wetting layer is observed in the vicinity of the silicon surface. This wetting layer sticks to the silicon surface and possibly does not move with the bulk ferrofluid. The wetting layer consists of layers # 1-3. Layer # 1 again contains ligand material and water and has a thickness of (3.2±0.5) nm. This thickness is in good agreement with the thickness of layer # 1 in all other cases and probably matches the length of the double shell of ligands. It is noticeable that its roughness of 0.5 nm is smaller than that obtained in all other cases. This result points toward a better defined layering of the system under shear. From the fits to the data an SLD value of $Nb_{\#\,1} = 1.12 \cdot 10^{-4}\text{nm}^{-2}$ was determined which is slightly higher compared to the static case and can be explained by a slightly higher water content and less excess oleic acid than in the static case.

Under shear, the thickness of layer # 2 was determined to be 15.0 nm which is 38 % higher. Also the SLD has a higher value of $Nb_{\#\,2} = 3.17 \cdot 10^{-4}\text{nm}^{-2}$. The larger thickness of layer # 2 can be explained as a less densely packed layer compared to the static case and it is not just a well-defined, single layer of particles. Such a scenario would have a higher SLD in the layer due to more water, as is observed. However, this situation would likely result in a higher roughness, which was not observed from the fits to the data. As in the static case, the roughness was found to be ±1.1 nm.

In the case of shear the thickness of layer # 3 was determined to be (2.8±1.4) nm which roughly corresponds to the bilayer shell thickness. This value is smaller compared to the

results obtained in all of the static cases. Since the SLD of layer # 3 is larger than that obtained in the static cases, it appears that this layer contains more water. The shear-induced changes in layer # 3 have to be discussed within the context of the entire structure, taking into account layer # 4. As mentioned above, it can be assumed that in the case of shear, both a static wetting layer and a moving ferrofluid occurs. Therefore, layer # 3 contains only the ligands of the static wetting layer.

Layer # 4 has a thickness of (12.2±3.2) nm which roughly corresponds to the average core size. Its SLD is $Nb_{\#\,4} = 5.14 \cdot 10^{-4}\mathrm{nm}^{-2}$, which is higher than the SLDs of both the transition region and the ferrofluid-bulk. An increased SLD in the case of shear can be explained by a higher water content with respect to the SLDs of the transition region and the ferrofluid bulk and therefore probably means depletion of oleic acid coated Fe_2O_3 particles relative to the bulk ferrofluid. It corresponds to the formation of a layer between the static wetting layer and the moving ferrofluid.

4 Summary

In summary, reflectometry measurements of a ferrofluid in contact with a silicon surface and exposed to different conditions of shear and magnetic field were performed. In all cases, a densely packed wetting layer builds up at the silicon surface. In the static case without shear the core part of the wetting layer very much agrees in thickness with the average core size of the particles. Supported by simple geometrical model calculations, the wetting layer can be assumed to be a densely packed sheet of particles. The observed ordering is predominantly one dimensional, as induced by surface interactions and it is limited to a very short distance from the surface. In the plane, any reference to close packing is strictly from a density point of view. We do not determine long range order in our measurements, only that there is sufficient short range order to support the packing densities that we observe. Beyond the short near-surface region, the ferrofluid appears to be evenly dispersed. When wetting the surface, the bilayer shell around the particles stays intact leading to a distance of two bi-layers between the particles in the densely packed wetting layer. The ferrofluid solution contains enough excess oleic acid to completely wet the silicon surface and to eliminate most of the water from the layers close to the surface. The hybrid layer that forms at the SiO_2 interface includes the oleic acid that coats the substrate surface along with ligands that form a shell around the nanoparticles. Since this hybrid layer does not change substantially upon shearing the ferrofluid or applying a magnetic field, we conclude that it is essential for stabilizing the wetting layer, presumably via steric interactions. This base layer facilitates the growth of a second nanoparticle layer, not as densely packed and not as ordered as the wetting layer, which is assumed to build up between the wetting layer and the ferrofluid bulk which is assembled at a depth of 60 nm from the silicon surface.

When a magnetic field is applied, shape anisotropy induces a torque that acts on the elongated particles and gradually aligns them with their longer axes parallel to the silicon surface. This nanoparticle rotation leads to a smaller core layer thickness and a higher packing density. The SLD value is correspondingly higher. Also for this case, the second nanoparticle layer again forms but the distance between the two nanoparticle layers is greater than that observed in the zero-field case. We speculate that the nanoparticle reorientation leads to changes in the dipole interactions among the nanoparticles which then results in a greater repulsion between the layers[21].

In the case of shear a static densely-packed particle layer at the interface and a moving bulk ferrofluid can be assumed. Due to shear the wetting layer is slightly spread out in thickness which can be explained by the assumption that the wetting layer is very stable and only immobile particles stick to the silicon surface. Between the moving ferrofluid and the static wetting layer, a depletion layer occurs as a result.

We have demonstrated that the interactions between a ferrofluid and a solid interface lead to the formation of self-assembled, multilayer structures. The hybrid organic layer that forms on the substrate surface appears to stabilize the complex wetting layer even in the presence of shear. The composition and thickness of the individual layers are sensitive to nanoparticle size and shape distributions as a result of the competing energetic interactions in the system. Application of a magnetic field leads to subtle variations in the layer characteristics. These results thus provide a path forward for controlling and tuning these self-assembled structures for device applications.

Additional experiments are needed to determine the role of the surface properties such as hydrophobicity etc., on the ordering in more detail. In addition, ordering at magnetic or patterned surfaces or temperature may be employed to determine the interaction strength of the particles in the layers.

5 Acknowledgments

We gratefully acknowledge financial support by ILL Grenoble, NIST Gaithersburg and University of Applied Sciences Bremerhaven. We thank Nadine Mill, University of Bielefeld, Germany for performing TEM measurements. We also thank Avi Saini from Uppsala University, Paul Kienzle, Kathryn Krycka, Cindi Dennis from NIST for fruitful discussions and Brian Maranville, Sushil Satija, Frank Henrich and David Hoogerheide for assistance with complementary measurements performed on the MAGIK and NG7 reflectometers at the NCNR.

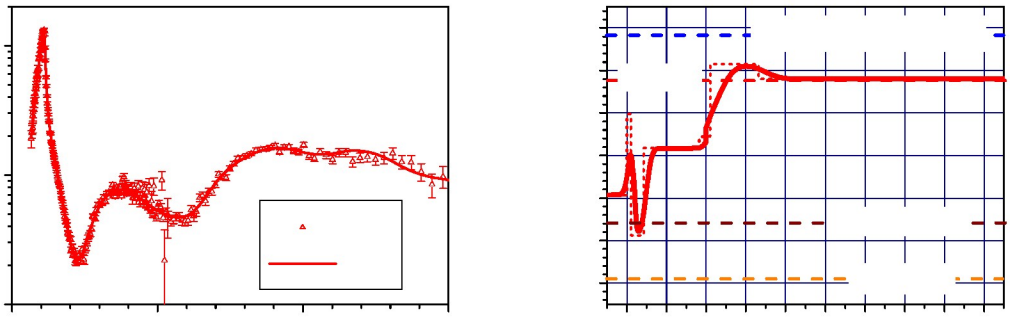

Fig. 10 (Color online) NR data taken under shear without applying a magnetic field. The fluid was pumped through the flow cell with a volumetric flow rate of $Q = 1000$ ml/min corresponding to a shear rate of $\dot{\gamma} = 313\ s^{-1}$. The solid lines represent fits to the data. Right: Profile of nuclear scattering length density plotted as function of distance from the Si(100) surface determined from results of the least square fitting routines applied to the reflectivity curves.

References

1 R. E. Rosensweig, Ferrohydrodynamics (Cambridge University Press, Cambridge, England, 1985).
2 E. Blums, A. Cebers, and M. M. Maiorov, Magnetic Fluids (de Gruyter, Berlin, 1997).
3 Schmidt, Benkoski, Cavicchia and Karim, Soft Matter **7**, 5756 9 (2011).
4 B. Berkovsky, V. Bashovoy, Magnetic Fluids and Applications Handbook (Begell House, New York, 1996).
5 H. Shahnazian, D. Gräf, D.Yu. Borin, and S. Odenbach, J. Phys. D: Appl. Phys. **42**, 205004 (2009).
6 I. Torres-Daz and C. Rinaldi, Soft Matter **10**, 8584 (2010).
7 A. Wiedenmann, A. Hoell, M. Kammel, and P. Boesecke, Phys. Rev. E **68**, 031203 (2003).
8 A. Wiedenmann, M. Kammel, A. Heinemann, and U. Keiderling, J. Phys.: Condens. Matter **18**, 2713 (2006).
9 A. Wiedenmann and A. Heinemann, J. Magn. Magn. Mater. **289** 58, (2005).
10 J. B. Hayter, J. Appl. Cryst. **21**, 737 (1988).
11 S. Hess, in Physics of Complex and Supramolecular Fluids, ed. by S.A. Safran, N.A. Clark (Wiley, New York, 1987), pp. 631642.
12 S. Hess, M. Weider, and M. Kröger, Magnetohydrodynamics **37** 287 (2001).
13 J.P. McTague, J. Chem. Phys **51**, 133 (1969).
14 W. F. Hall and S. N. Busenberg, J. Chem. Phys. **51** 137 (1969).
15 M. I. Shliomis Sov. Phys., JETP **34** 1291 (1972).
16 L.M. Pop and S. Odenbach, J. Phys.: Condens. Matter **18**, 2785 (2006).
17 P. Ilg, M. Kroeger, and S. Hess, J. Magn. Magn. Mater **289**, 325 (2005).
18 C.Y. Matuo, A. Bourdon, A. Bee, and A. M. Figueiredo Neto, Phys. Rev. E **56**, R1310 (1997).
19 G. Barbero, A. Bourdon, A. Bee, and A. M. Figueiredo Neto, Phys. Lett. A **259**, 314 (1999).
20 I. Takahashi, N. Tanaka, and S. Doi, J. Appl. Cryst. **36**, 244 (2003).
21 A. Vorobiev, J. Major, H. Dosch, G. Gordeev, and D. Orlova, Phys. Rev. Lett. **93**, 267203 (2004).
22 B. M. Berkovsky, V. F. Medvedev, and M. S. Krakov, Magnetic Fluids; Engineering Applications (Oxford University Press, Oxford, 1993).
23 The ferrofluid used was supplied by Liquids Research Limited
24 Information given by the supplier.
25 ImageJ userguide, http://rsbweb.nih.gov/ij/docs/userguide.pdf
26 D. van der Grinten, M. Wolff, H. Zabel, A. and Magerl, Meas. Sci. Technol. **19**, 34016 (2008).
27 B.P. Toperverg, in: Th. Brückel and W. Schweika (Eds.), Polarized Neutron Scattering, Jülich Series "Matter and Materials", **12**, 249 (2002).
28 H. Zabel, K. Theis-Bröhl, B. Toperverg, Polarized neutron reflectivity and scattering of magnetic nanostructures and spintronic materials, In Handbook of Magnetism and Advanced Magnetic Materials by H. Kronmüller/ S. Parkin (Eds.), Wiley p. 1237 (2007).
29 Charles F. Majkrzak, Christopher Metting, Brian B.

Maranville, Joseph A. Dura, Sushil Satija, Terrence Udovic, and Norman F. Berk, Physical Review A 89, 033851 (2014).
30 R. Cubitt and G. Fragneto, Appl. Phys. A **74**, 329 (2002).
31 L. G. Parratt, Phys. Rev. **95**, 359 (1954).
32 S.C. DeCaluwe et al., Soft Matter **10**, 5763 (2014).
33 P.A. Kienzle, K.V. O'Donovan, J.F. Ankner, N.F. Berk, C.F. Majkrzak; http://www.ncnr.nist.gov/reflpak. 2000-2006
34 D. Mishra, M. J. Benitez, O. Petracic, G. A. Badini Confalonieri, P. Szary, F Brüssing, K. Theis-Bröhl, A. Devishvili, A. Vorobiev, O. Konovalov, M. Paulus, C. Sternemann, B. P. Toperverg and H. Zabel, Nanotechnology **23**, 055707 (2012).
35 NIST Scattering Length Density Calculator http://www.ncnr.nist.gov/resources/sldcalc.html